COMMUNICATION

Two-step Thermal Annealing: An Effective Route for 15% Efficient Quasi-2D Perovskite Solar Cells

Valentino Romano,[a]⊥ Leyla Najafi,[b,c]⊥, Albertus Adrian Sutanto [d]⊥, Giorgio Schileo,[e]⊥ Valentin Queloz,[d] Sebastiano Bellani,[b,c] Mirko Prato,[f] Sergio Marras,[f] Mohammad Khaja Nazeeruddin,[d]* Giovanna D'Angelo,[a] Francesco Bonaccorso[b,c] and Giulia Grancini[e]*

⊥ These authors have equally contributed to the work

[a] Dr. V. Romano, Prof. G. D'Angelo
Department MIFT
University of Messina
Viale F. Stagno d'Alcontres 31, S. Agata, 98166 Messina, Italy
[b] Dr. L. Najafi, Dr. S. Bellani, Dr. F. Bonaccorso
Graphene Labs
Istituto Italiano di Tecnologia
Via Morego 30, 16163 Genova, Italy
[c] Dr. L. Najafi, Dr. S. Bellani, Dr. F. Bonaccorso
BeDimensional Spa.,
Via Lungotorrente Secca 3D, 16163 Genova, Italy
[d] A. A. Sutanto, V. Queloz, Prof. M. K. Nazeeruddin
Group of molecular Engineering of Functional Materials, Institute of Chemical Sciences and Engineering
École Polytechnique Fédérale de Lausanne
Valais Wallis, Rue de l'Industrie 17, Sion CH-1951
[e] Dr. G. Schileo, Prof. G. Grancini
Department of Chemistry and INSTM,
University of Pavia
Via Taramelli 14, 27100 Pavia, Italy
E-mail: giulia.grancini@unipv.it
[f] Dr. M. Prato, Dr. S. Marras
Materials Characterization Facility
Istituto Italiano di Tecnologia
Via Morego 30, 16163 Genova, Italy

Supporting information for this article is given via a link at the end of the document.

Abstract: Low-dimensional perovskites (LDP) are nowadays recognized as promising materials for the realization of highly performing photovoltaic cells. However, issues related to film morphology, composition, crystal quality and material homogeneity limit the device performances and reproducibility. In this work, we implement a robust method for the deposition of a LDP mixing methylammonium (MA) and phenylethylammonium (PEA) cations to create the mixed system $(PEA)_2MA_{39}Pb_{40}I_{121}$ by using a two-step thermal annealing treatment (at 60 and 100 °C). Our approach results in LDP films with high crystal quality and enhanced carrier lifetime, which double the power conversion efficiency of reference devices, reaching up to 15%.

Perovskite solar cells (PSCs) represent a cutting-edge technology in PVs due to their cost-effectiveness, ease of fabrication through solution-based processes, and high performances, leading nowadays to power conversion efficiencies (PCE) beyond 25%.[1–4] In general, three-dimensional (3D) perovskites are ionic materials with chemical formula ABX_3, where A and B are cations, while X is an anion.[3,5,6] The crystalline structure of such compounds is characterised by corner-sharing $(BX_6)^{4-}$ octahedra, with the A^+ occupying the cavity formed by this periodic pattern.[3,5,6] More recently, significant research effort has been focused on the development of LDP, also known as two-dimensional (2D) perovskites,[7,8] characterised by different lattice arrangements from their 3D counterparts, such as the Ruddlesden-Popper (RP) phase with chemical formula of R_2BX_4.[9–12] More in details, RP perovskites comprise large hydrophobic organic cations R^+ that do not fit the cavities formed by the $(BX_6)^{4-}$ octahedra. As a result, RP perovskites show a layered structure made up by single layers of $(BX_6)^{4-}$ octahedra sandwiched between two layers of R^+ cations.[7,9] Such low-dimensional structure leads to quantum confinement effects responsible for a plethora of unique physical and chemical properties, including strong exciton binding energy (> 300 meV)[13–15] and high photoluminescence quantum yield (>5%).[16,17] However, such properties might limit charge generation efficiency and transport thereof, making their use as active materials in solar cells critical.[9] Alternatively, if a suitable A^+ cation (*e.g.*, methyl-ammonium (MA), formamidinium, and Cs) is added into the RP structure, quasi -2D perovskites are obtained. These have chemical formula $R_2A_{n-1}B_nX_{3n+1}$, where *n* is the number of inorganic $(BX_6)^{4-}$ layers held together by the A^+ cation.[9] Notably, the band gap decreases with increasing *n,* extending the use of this class of materials into efficient light antennas and charge transport layers.[9,18,19]

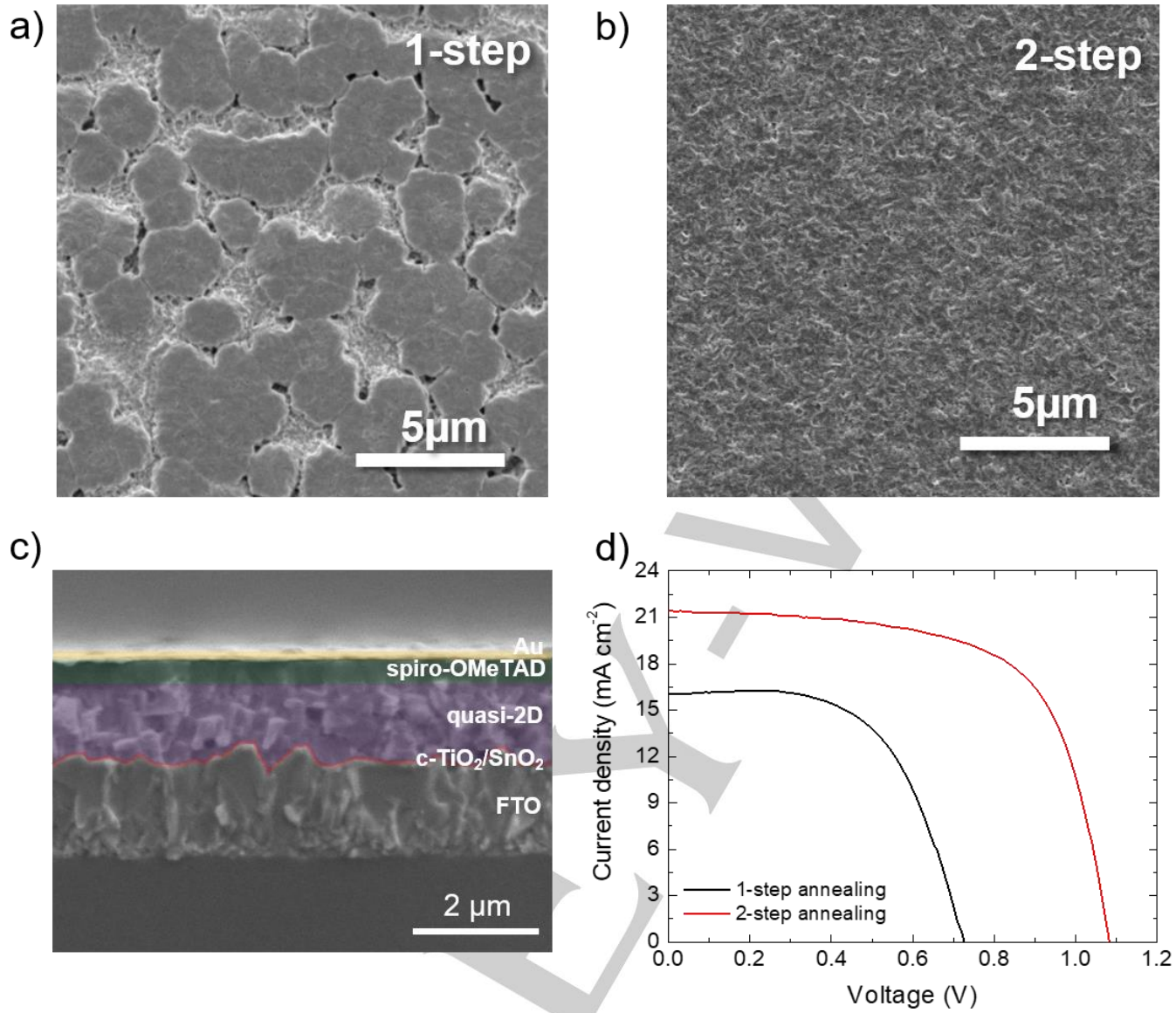

Figure 1. Top-view SEM image of $(PEA)_2(MA)_{39}Pb_{40}I_{121}$ quasi-2D perovskite prepared through a) 1-step annealing and b) 2-step annealing process. c) Cross-sectional SEM image of the PSC architecture. All the different layers composing the device architecture can be resolved (the estimated thickness of the quasi-2D perovskite layer is ~520 nm) except the SnO_2 layer, whose thickness (~10 nm) is significantly inferior to the ones of the other layers. d) Comparison of the J-V curves (reverse scan) for the best performing devices obtained by using 1-step (black line) and 2-step (red line) thermal treatment for the quasi-2D perovskite layer.

When integrated in PSCs, high PCE have been obtained (> 12%), depending on the different R^+ organic spacers used or the *n* values. In particular, PCE values range from 15.42% with 2-thiophenemethylammonium (*n* = 3),[20] to > 18% with benzylammonium (*n* = 9),[21] 3-bromobenzylammonium (3 < *n* < 4) [22] butylammonium and guanidinium (*n* = 6),[23] up to 18.5% with phenylethylammonium (*n* = 4).[24,25] Unfortunately, no common reproducible protocols have been obtained so far, especially for high *n* values. Indeed, when *n* increases to 30, 40, a lack of control on material composition influences the reproducibility of the film, resulting in non-uniform device performances. Indeed, the use of the large R^+ cations (typically aliphatic or aromatic alkylammonium cations, *e.g.*, phenylethyl-ammonium (PEA) and *n*-butylammonium) makes the control of the crystal growth challenging, and no consensus on the deposition protocol of such materials has been achieved yet.[26] Thus, several strategies have been proposed with the aim to optimise the quality of the resulting photoactive thin-films, such as one-step spin coating,[13] sequential dipping[27] and spin coating,[28] hot-casting spin coating,[29] drop-casting on heated substrates,[30] gas flow-assisted drying of drop-casted films,[31] vapour deposition[32,33] and incorporation of additives in the precursor solution.[34] In this work, we optimize the process for the deposition of quasi-2D perovskites through the engineering of the precursor solution solvent and the design of an effective annealing procedure. In particular, we chose $(PEA)_2MA_{39}Pb_{40}I_{121}$ (*i.e.*, *n* = 40,) as perovskite absorber and investigated three different solvents in the precursor solution. We found that a crucial factor for the deposition of the quasi-2D perovskite is the engineering of a co-solvent approach and a 2-step annealing treatment of the perovskite layer: using a 50:50 mixture of dimethyl sulfoxide (DMSO): γ-Butyrolactone (GBL) and annealing the film sequentially at 60 °C for 2 min and then at 100 °C for 1 h. In particular, the second annealing step is essential for the formation of thin-films with a homogeneous morphology, reducing the pinholes density and improving the overall quality of the material.

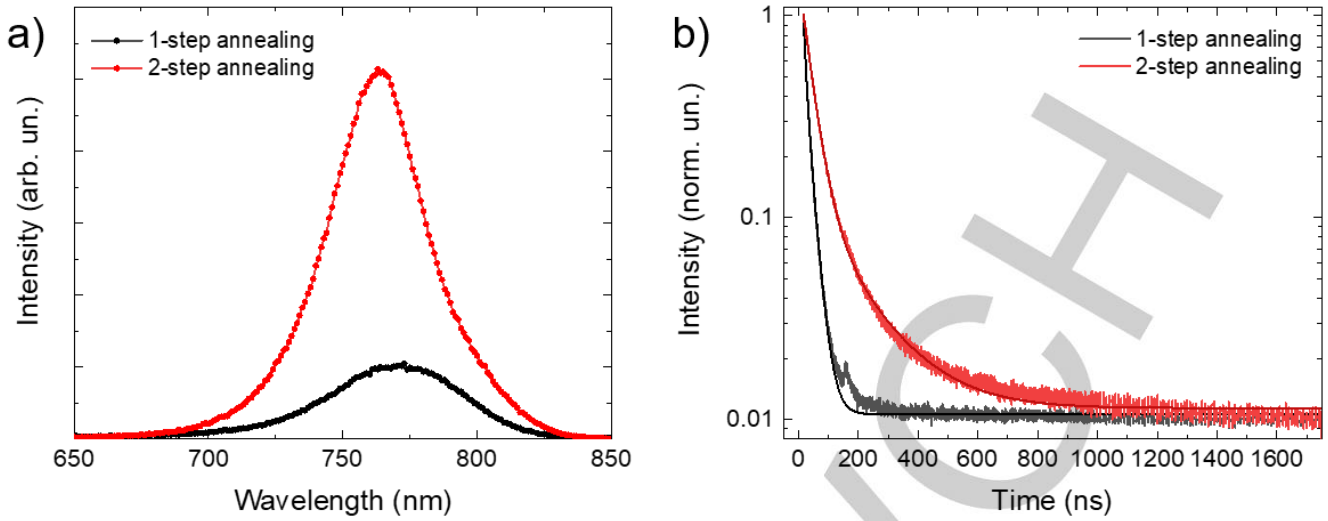

Figure 2. a) Photoluminescence spectrum with a 450nm excitation of the 1- and 2-step annealing. b) Photoluminescence decay at 770nm with a 635nm excitation with biexponential decay fit (solid line).

Different solvents have been also tried, leading to device performances poorer than those obtained using DMSO:GBL mixture. These results are likely explained by considering the different vapor pressure and boiling point of the investigated solvents, which influence the crystallization process of the perovskite films (see further discussion in the Supplementary Information and **Figure S1**). The perovskite precursor solution was prepared by dissolving PEAI, MAI and PbI_2 according to the molecular formula $(PEA)_2(MA)_{39}Pb_{40}I_{12}$, at 2 M PbI_2 concentration, as described in similar literature protocols.[15,16,19]

The so-produced solution was deposited in a N_2-filled glove box following a 2-step deposition process (see Experimental Section in the supporting information for details) and using the common "anti-solvent" method to control the crystallization of the perovskite,[35] resulting in dense and crystalline perovskite thin film. Subsequently, we annealed the film at 100 °C for 1 h, adopting 1-step annealing approach, as defined by standard procedure for high efficient solar cells.[2] The resulting film morphology was investigated through scanning electron microscopy (SEM). As shown in **Figure 1a**, the morphology of the film is characterized by rounded domains which lack of a continuous interconnection and form large density of pinholes. Such discontinuous morphology is ascribed to the relatively fast nucleation rate of the perovskite crystallites, leading to inhomogeneities on a microscopic scale.[36] To improve the film morphology and maximise the device performance, we engineered the annealing process by implementing a second slower annealing step. More in details, firstly, the films were placed at 60 °C for 2 min (until the absorber layer turned dark), and then at 100 °C for 1 h. This 2-step annealing resulted in the formation of thin films with a homogeneous surface coverage, dense and interconnected morphology without the presence of any pinhole (**Figure 1b**) even on the cross section (**Figure 1c**). To assess the effects of the perovskite film morphology on device performances, hybrid *n-i-p* planar PSCs were produced (see more details in Supporting Information) using either 1-step and the 2-step annealing protocols. **Figure 1c** shows a cross-sectional SEM image of a representative device, evidencing its layered architecture composed of FTO/compact TiO_2 (c-TiO_2)/SnO_2/quasi-2D perovskite/2,2(7,7)-tetrakis-(N,N-dipmethoxyphenylamine)9,9(-spirobifluorene) (spiro-OMeTAD)/Au. **Figure 1d** reports the current density - voltage (J-V) curves of the devices produced using 1-step and 2-step annealing procedures, as described above. **Table 1** summarizes the PV parameters derived from the corresponding J-V curves.

Table 1. PV parameters of the two best-performing quasi-2D-perovskite-based devices, measured at 1 sun (AM 1.5G) illumination, prepared with the 1-step and 2-step annealing treatments, respectively.

SAMPLE	J_{SC} [mA cm^{-2}]	V_{OC} [V]	FF [%]	PCE [%]
1-step annealing	16.00	0.73	59.4	6.90
2-steps annealing	21.41	1.08	65.05	15.07

Noteworthy, the 2-step annealing procedure led to a significant increase in the performance of the devices, which reached PCE up to 15.07%. This value corresponds to a 118% enhancement compared to the PCE of the device produced with the 1-step annealing. The improvement of the PCE in the 2-step annealed device is associated to the maximization of both the short-circuit current density (J_{SC}) (21.41 mA cm^{-2}) and the open-circuit voltage (V_{OC}) (1.08 V). The reproducibility of the obtained performances was confirmed by statistical analysis of the photovoltaic parameters measured for different devices for each configuration, as shown in **Figure S1b**. The superior photovoltaic performances of the cells produced using the 2-step annealing treatment, compared to those fabricated with the 1-step annealing procedure, are ascribed to the morphology differences of the quasi-2D perovskite films, as shown in **Figure 1a, b**. In particular, the uniform and pinhole free perovskite layer formed by 2-step annealing process improves the charge collection and reduces the undesired recombination path, as evident by the higher V_{OC}, J_{SC} and FF.[36–39] To rationalize the origin of the different performances, we monitored the optical properties of the quasi-2D perovskite films by means of UV-Vis absorption spectroscopy and steady-state and transient photoluminescence (PL) measurements. As shown in **Figure S2a**, the UV-Vis absorption spectrum of the quasi-2D perovskite film resembles the one measured for the 3D case (*i.e.*, $MAPbI_3$), in agreement with the high *n* of our quasi-2D perovskite (*n* = 40).[9,13,15]

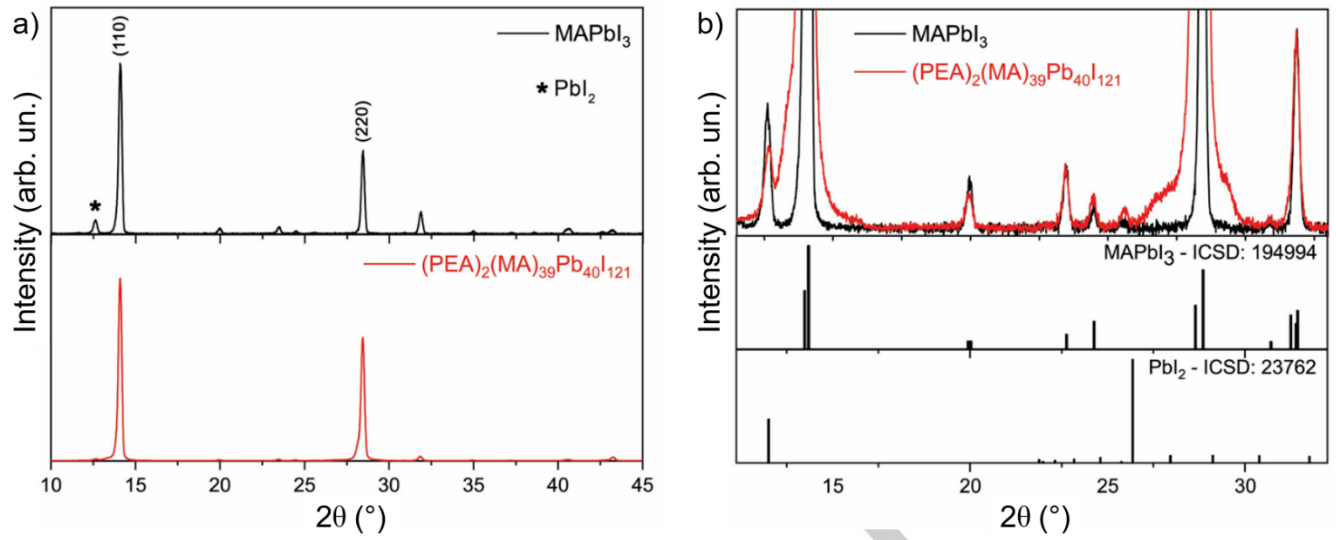

Figure 3. a) XRD patterns of $MAPbI_3$ (black line) and $(PEA)_2(MA)_{39}Pb_{40}I_{121}$ (red line). b) Zoomed XRD patterns of the investigated perovskites, together with the corresponding ICSD cards' peak of $MAPbI_3$ and PbI_2.

By analysing the Tauc plot (*i.e.*, $(\alpha h\nu)^n$ *vs.* hν) using the Tauc relation $Ah\nu = Y(h\nu - E_g)^2$ for direct-allowed transition materials (E_g is the optical band gap, A is the absorbance, h is Planck's constant, ν is the photon's frequency, and Y is a proportionality constant),[40] the E_g of the quasi 2D perovskite films produced with 1-step and 2-step annealing treatments were 1.60 eV (~775 nm) and 1.61 eV (~770 nm), respectively (**Figure S2b,c**). Therefore, no significant differences in the E_g are observed between quasi-2D and 3D perovskites, as commonly observed in previous literature for high n quasi-2D perovskites.[9,13,15] **Figure 2a** shows the steady-state PL spectra of the two samples. The quasi 2D-perovskite film prepared with the 2-step annealing method shows a more intense PL signal than the one of the quasi-2D perovskite film prepared with 1-step annealing procedure. Despite this measurement does not pretend to be quantitative, it shows that, at same experimental conditions, the PL signal is significantly more intense for the optimized 2-step annealing thin film. **Figure 2b** reports the transient PL measurements on the same set of samples. We observe that the PL signal for the 2-step annealed film is longer living compared to the sample prepared by the 1-step process, suggesting a longer lifetime for the photogenerated charges in the former quasi-2D perovskite film with respect to the latter. From the fit of the PL data (see Supporting Information for more details on the fitting procedure) the main time constant elongates from τ_1=8 ns to τ_1=34 ns comparing 1-step annealed to 2-step annealed film, respectively. The enhancements of the PL intensity and the longer living PL signal in the 2-step annealing treatment indicate that charges have a longer lifetime (compared to the sample prepared with the 1-step protocol), suggesting the reduction of non-radiative recombination paths. This also explains the higher V_{oc} and J_{sc} observed in the compared devices.

To further analyse the structure of the optimized quasi-2D perovskite film, we performed X-ray diffraction (XRD) measurements to analyse the crystalline structure of the sample, as well as its crystal orientation. The XRD pattern of the quasi-2D perovskite shows two main peaks at 2θ = 14.1° and 28.4° (**Figure 3a**), which are associated to the (110) and (220) reflections of the tetragonal perovskite phase for $MAPbI_3$ with *I4cm* space group (**Figure 3a**). The strong intensity of these peaks confirms the crystalline nature of our samples and, in addition, highlights the high preferential orientation of crystalline domains along the crystallographic direction [110] and consequently the presence of inorganic planes of PbI_6 parallel to the substrate. From the comparison with the XRD pattern of the $MAPbI_3$, it is evident that the preferential orientation of crystalline domains is definitely more pronounced in the quasi-2D perovskite. The zoomed range in **Figure 3b** shows the other weak peaks of the perovskite structure. The angular position of those peaks is equivalent for both quasi-2D perovskite and $MAPbI_3$, indicating that they share the same crystal structure. The same crystal structure for $MAPbI_3$ and quasi-2D perovskite is consistent with previous reports,[13,15,16] which is ascribed to the high n chosen for the quasi-2D formulation (n = 40). Trigonal PbI_2 (*P3m1* space group) is another phase typically formed as by product during perovskite synthesis. A comparison of the XRD patterns of the quasi-2D perovskite and $MAPbI_3$ reveals that the PbI_2 quantity present in the quasi-2D perovskite can be considered almost negligible compared to that observed in the $MAPbI_3$ sample. In order to identify further distinctive properties of the as-produced quasi-2D perovskite compared to the $MAPbI_3$ reference, X-ray photoelectron spectroscopy (XPS) measurements were carried out to provide information about the chemical composition of the samples.[15,16] The data collected over the binding energy regions typical for I 3d, N 1s, C 1s and Pb 4f XPS peaks are shown in **Figure 4** and compared to those acquired on the $MAPbI_3$ reference. The data show a clear similarity between $(PEA)_2(MA)_{39}Pb_{40}I_{121}$ and $MAPbI_3$ spectra, with the main peaks appearing at close binding energy positions, as reported in **Table 2**. This indicates that the chemical environment of iodine, nitrogen, carbon and lead in the quasi-2D perovskite resembles that in a pure 3D counterpart, as expected for the chosen n value (n = 40). However, the quantitative analysis brought to light some differences between the stoichiometries of the two samples. In particular, the $(PEA)_2(MA)_{39}Pb_{40}I_{121}$ sample is characterized by slightly higher N/Pb and I/Pb ratios compared to the 3D reference, in line with the expected stoichiometry. To elucidate the stability of the quasi-2D perovskite films, we have performed absorbance and XRD measurements on fresh and aged (after 7 and 14 days) samples. Our assessments were performed on three different perovskites: quasi-2D perovskite films produced by 1-step and 2-

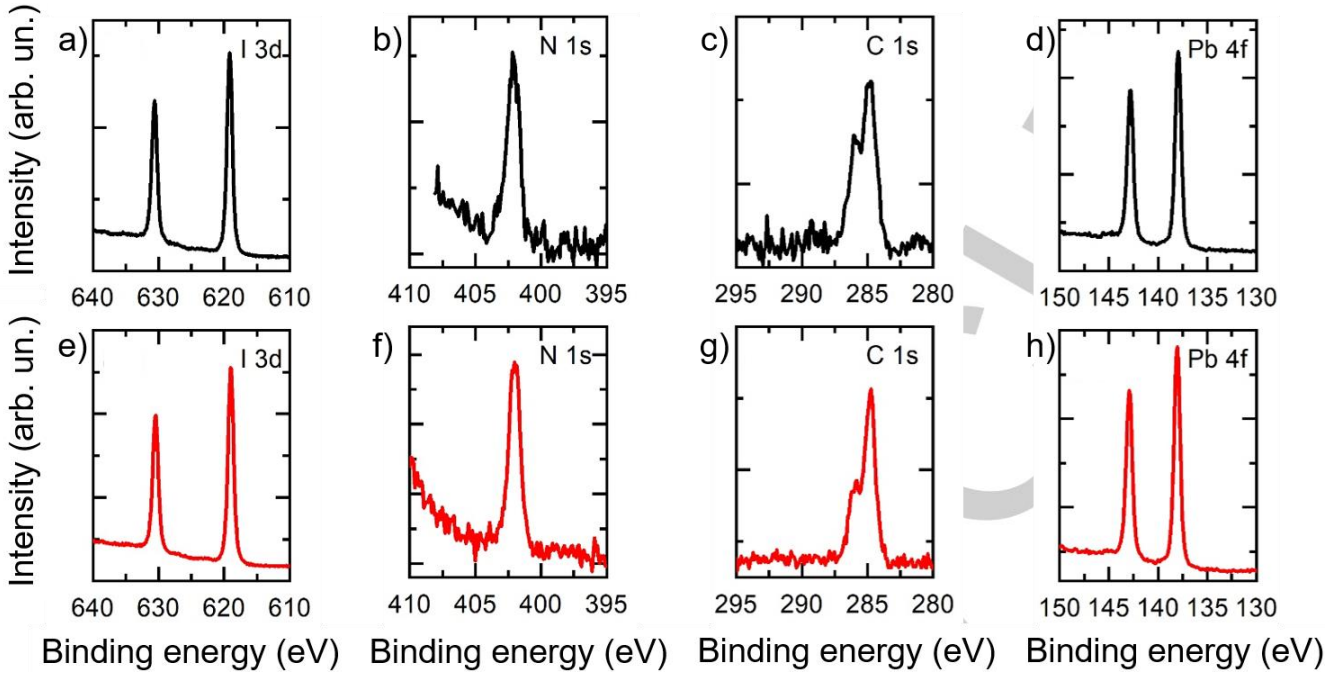

Figure 4. Representative XPS data collected on $MAPbI_3$ (black line) and $(PEA)_2(MA)_{39}Pb_{40}I_{121}$ (red line) films, over the energy regions typical for I 3d (panels a and e), N 1s (panels b and f), C 1s (panels c and g), and Pb 4f (panels d and h) peaks.

step annealing, and a $MAPbI_3$ reference film. All films were aged in dark under a controlled humidity (RH<40%) without any encapsulation. The absorbance and XRD spectra are shown in **Figure S3**. The absorbance spectra do not show significant variations upon aging, exhibiting the same absorbance onset (**Figure S3a-c)**. The XRD spectra (**Figure S3d-f**) show that both 1-step and 2-step annealing quasi-2D perovskites maintain the initial low PbI_2 content over time (peak denoted by "*"). Differently, the $MAPbI_3$ film shows an increase of the PbI_2 content over time, indicating a chemical instability compared to the quasi-2D perovskites.[15] Lastly, the J-V curve of the best performing device prepared using the 2-step annealing quasi-2D perovskite film was measured after 168 h. As shown in **Table S3**, the device exhibited a high PCE retention (~88%) over 168 h after its fabrication. Prospectively, the engineering of the device architecture may further improve the stability of the device based on quasi-2D perovskite produced by 2-step annealing procedure.

Table 2. Binding energy positions of the main XPS peaks for $MaPbI_3$ and quasi-2D perovskites.

SAMPLE	I 3d [eV]	N 1s [eV]	C 1s (C-N) [eV]	Pb 4f [eV]
$MAPbI_3$	619.2±0.2	402.1±0.2	286.0±0.2	138.0±0.2
$(PEA)_2(MA)_{39}Pb_{40}I_{121}$	619.2±0.2	402.0±0.2	286.0±0.2	138.0±0.2

In summary, our work demonstrates an innovative and robust method for the realization of high quality quasi-2D perovskites with uniform morphology, and their integration in solar cells with PCE over 15%. Our crucial observation if that the optimization of the crystal growth rate – slowing it down – is essential for a proper nucleation of the quasi-2D perovskite and for obtaining high quality thin films. Our investigations define the protocol for the deposition conditions of quasi-2D perovskite with $n = 40$ and using PEAI. The protocol requires the use of a 50:50 volume ratio of DMSO:GBL as solvent mixture, an initial PbI_2 concentration of 2 M and a 2-step annealing treatment. By using these optimized parameters, PCE as high as 15.07% for *n-i-p* planar perovskite solar cell has been reached. The optimization of the film quality and device performances are ascribed to the reduced non-radiative recombination processes, associated to a homogeneous crack-free morphology, in the quasi-2D perovskite films treated by 2-step annealing, in comparison to the 1-step annealed ones. These results underline the importance of defining a robust protocol and reproducible experimental conditions for the realization of quasi-2D perovskite solar cells with elevated *n*, filling the existing gap in literature and providing a new optimization route to follow.

Acknowledgments

This project has received funding from the European Union's Horizon 2020 research and innovation program under grant agreement No.785219 and No. 881603-GrapheneCore2 and GrapheneCore3. This project has received funding from European Union's MSCA-ITN ULTIMATE project under grant agreement No. 813036 and from the Italian Ministry of Foreign Affairs and International Cooperation (MAECI) through Cooperation Project "GINGSENG" (Grant PGR05249>) between Italy and China. G.S. and G.G. acknowledge the "HY-NANO" project that has received funding from the European Research Council (ERC) Starting Grant 2018 under the European Union's Horizon 2020 research and innovation programme (Grant agreement No. 802862).

Keywords: crystal growth • perovskites • solar cells • thermal annealing • thin films

References

[1] "National Renewable Energy Laboratory," can be found under https://www.nrel.gov/pv/cell-efficiency.html, **n.d.**

[2] M. Saliba, J. P. Correa-Baena, C. M. Wolff, M. Stolterfoht, N. Phung, S. Albrecht, D. Neher, A. Abate, *Chem. Mater.* **2018**, *30*, 4193–4201.

[3] J. P. Correa-Baena, M. Saliba, T. Buonassisi, M. Grätzel, A. Abate, W. Tress, A. Hagfeldt, *Science (80-.).* **2017**, *358*, 739–744.

[4] J. P. Correa-Baena, A. Abate, M. Saliba, W. Tress, T. Jesper Jacobsson, M. Grätzel, A. Hagfeldt, *Energy Environ. Sci.* **2017**, *10*, 710–727.

[5] M. I. H. Ansari, A. Qurashi, M. K. Nazeeruddin, *J. Photochem. Photobiol. C Photochem. Rev.* **2018**, *35*, 1–24.

[6] M. Saliba, J. P. Correa-Baena, M. Grätzel, A. Hagfeldt, A. Abate, *Angew. Chemie - Int. Ed.* **2018**, *57*, 2554–2569.

[7] L. Mao, C. C. Stoumpos, M. G. Kanatzidis, *J. Am. Chem. Soc.* **2019**, *141*, 1171–1190.

[8] H. Kim, K. A. Huynh, S. Y. Kim, Q. Van Le, H. W. Jang, *Phys. Status Solidi - Rapid Res. Lett.* **2020**, *14*, 1900435.

[9] G. Grancini, M. K. Nazeeruddin, *Nat. Rev. Mater.* **2019**, *1*.

[10] D. B. Mitzi, *Prog. Inorg. Chem.* **2007**, *48*, 1–121.

[11] S. Ahmad, P. Fu, S. Yu, Q. Yang, X. Liu, X. Wang, X. Wang, X. Guo, C. Li, *Joule* **2019**, *3*, 794–806.

[12] Y. Chen, Y. Sun, J. Peng, J. Tang, K. Zheng, Z. Liang, *Adv. Mater.* **2018**, *11*, 1703487.

[13] D. H. Cao, C. C. Stoumpos, O. K. Farha, J. T. Hupp, M. G. Kanatzidis, *J. Am. Chem. Soc.* **2015**, *137*, 7843–7850.

[14] C. C. Stoumpos, D. H. Cao, D. J. Clark, J. Young, J. M. Rondinelli, J. I. Jang, J. T. Hupp, M. G. Kanatzidis, *Chem. Mater.* **2016**, *28*, 2852–2867.

[15] L. N. Quan, M. Yuan, R. Comin, O. Voznyy, E. M. Beauregard, S. Hoogland, A. Buin, A. R. Kirmani, K. Zhao, A. Amassian, D. H. Kim, E. H. Sargent, *J. Am. Chem. Soc.* **2016**, *138*, 2649–2655.

[16] M. Yuan, L. N. Quan, R. Comin, G. Walters, R. Sabatini, O. Voznyy, S. Hoogland, Y. Zhao, E. M. Beauregard, P. Kanjanaboos, Z. Lu, D. H. Kim, E. H. Sargent, *Nat. Nanotechnol.* **2016**, *11*, 872.

[17] M. C. Weidman, A. J. Goodman, W. A. Tisdale, *Chem. Mater.* **2017**, *29*, 5019–5030.

[18] B. El Cohen, Y. Li, Q. Meng, L. Etgar, *Nano Lett.* **2019**, *19*, 2588–2597.

[19] B. El Cohen, M. Wierzbowska, L. Etgar, *Adv. Funct. Mater.* **2017**, *27*, 1604733.

[20] H. Lai, B. Kan, T. Liu, N. Zheng, Z. Xie, T. Zhou, X. Wan, X. Zhang, Y. Liu, Y. Chen, *J. Am. Chem. Soc.* **2018**, *140*, 11639–11646.

[21] H. Zheng, G. Liu, L. Zhu, J. Ye, X. Zhang, A. Alsaedi, T. Hayat, X. Pan, S. Dai, *Adv. Energy Mater.* **2018**, *8*, 1800051.

[22] R. Yang, R. Li, Y. Cao, Y. Wei, Y. Miao, W. L. Tan, X. Jiao, H. Chen, L. Zhang, Q. Chen, H. Zhang, W. Zou, Y. Wang, M. Yang, C. Yi, N. Wang, F. Gao, C. R. McNeill, T. Qin, J. Wang, W. Huang, *Adv. Mater.* **2018**, *30*, 1804771.

[23] X. Lian, H. Wu, L. Zuo, G. Zhou, X. Wen, Y. Zhang, G. Wu, Z. Xie, H. Zhu, H. Chen, *Adv. Funct. Mater.* **2020**, *30*, 2004188.

[24] Y. Yang, C. Liu, O. A. Syzgantseva, M. A. Syzgantseva, S. Ma, Y. Ding, M. Cai, X. Liu, S. Dai, M. K. Nazeeruddin, *Adv. Energy Mater.* **2020**, 2002966.

[25] Y. Yang, C. Liu, A. Mahata, M. Li, C. Roldán-Carmona, Y. Ding, Z. Arain, W. Xu, Y. Yang, P. A. Schouwink, A. Züttel, F. De Angelis, S. Dai, M. K. Nazeeruddin, *Energy Environ. Sci.* **2020**, *13*, 3093–3101.

[26] Z. Chen, Y. Guo, E. Wertz, J. Shi, *Adv. Mater.* **2019**, *31*, 1803514.

[27] T. M. Koh, V. Shanmugam, J. Schlipf, L. Oesinghaus, P. Müller-Buschbaum, N. Ramakrishnan, V. Swamy, N. Mathews, P. P. Boix, S. G. Mhaisalkar, *Adv. Mater.* **2016**, *28*, 3653–3661.

[28] N. Li, Z. Zhu, C. C. Chueh, H. Liu, B. Peng, A. Petrone, X. Li, L. Wang, A. K. Y. Jen, *Adv. Energy Mater.* **2017**, *7*, 1601307.

[29] H. Tsai, W. Nie, J. C. Blancon, C. C. Stoumpos, R. Asadpour, B. Harutyunyan, A. J. Neukirch, R. Verduzco, J. J. Crochet, S. Tretiak, L. Pedesseau, J. Even, M. A. Alam, G. Gupta, J. Lou, P. M. Ajayan, M. J. Bedzyk, M. G. Kanatzidis, A. D. Mohite, *Nature* **2016**, *536*, 312–316.

[30] C. Zuo, A. D. Scully, D. Vak, W. Tan, X. Jiao, C. R. McNeill, D. Angmo, L. Ding, M. Gao, *Adv. Energy Mater.* **2019**, *9*, 1803258.

[31] C. Zuo, A. D. Scully, W. L. Tan, F. Zheng, K. P. Ghiggino, D. Vak, H. Weerasinghe, C. R. McNeill, D. Angmo, A. S. R. Chesman, M. Gao, *Commun. Mater.* **2020**, *1*, 1–10.

[32] J. Wang, J. Zhang, J. Li, Q. Tan, L. Li, J. Zhang, J. Zang, P. Tan, D. Li, *J. Phys. Chem. Lett.* **2017**, *8*, 6211–6219.

[33] Z. Chen, Y. Wang, X. Sun, Y. Xiang, Y. Hu, J. Jiang, J. Feng, Y. Y. Sun, X. Wang, G. C. Wang, T. M. Lu, H. Gao, E. A. Wertz, J. Shi, *J. Phys. Chem. Lett.* **2018**, *9*, 6676–6682.

[34] X. Zhang, G. Wu, W. Fu, M. Qin, W. Yang, J. Yan, Z. Zhang, X. Lu, H. Chen, *Adv. Energy Mater.* **2018**, *8*, 1702498.

[35] Y. Zhou, M. Yang, W. Wu, A. L. Vasiliev, K. Zhu, N. P. Padture, *J. Mater. Chem. A* **2015**, *3*, 8178–8184.

[36] F. Hanush, M. Petrus, P. Docampo, in *Unconv. Thin Film Photovoltaics* (Eds: E. Da Como, F. De Angelis, H.J. Snaith, A. Walker), **2016**, pp. 32–56.

[37] W. Qiu, T. Merckx, M. Jaysankar, C. Masse De La Huerta, L. Rakocevic, W. Zhang, U. W. Paetzold, R. Gehlhaar, L. Froyen, J. Poortmans, D. Cheyns, H. J. Snaith, P. Heremans, *Energy Environ. Sci.* **2016**, *9*, 484–489.

[38] C. Fei, L. Guo, B. Li, R. Zhang, H. Fu, J. Tian, G. Cao, *Nano Energy* **2016**, *27*, 17–26.

[39] B. Li, J. Tian, L. Guo, C. Fei, T. Shen, X. Qu, G. Cao, *ACS Appl. Mater. Interfaces* **2016**, *8*, 4684–4690.

[40] J. I. Pankove, D. A. Kiewit, *J. Electrochem. Soc.* **1972**, *5*, 156C.

Entry for the Table of Contents

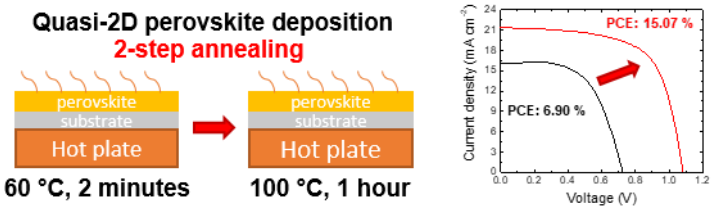

The use of quasi-2D perovskites as light harvesters is a promising route towards stable and efficient photovoltaics. Herein, we investigate the $(PEA)_2MA_{39}Pb_{40}I_{121}$ composition, showing that a 2-step annealing process promotes the formation of a homogeneous perovskite film. The latter is characterized by reduced radiative recombination rates and superior performances compared to perovskite films produced by 1-step thermal treatment.